

# Crystallographic and kinetic investigations of the covalent complex formed by a specific tetrapeptide aldehyde and the serine protease from *Streptomyces griseus*

(inhibitor/conformational change/transition state analogue)

GARY D. BRAYER\*, LOUIS T. J. DELBAERE\*, MICHAEL N. G. JAMES\*, CARL-AXEL BAUER†, AND ROBERT C. THOMPSON‡

\*Medical Research Council Group on Protein Structure and Function, Department of Biochemistry, University of Alberta, Edmonton, Canada, T6G 2H7; †Department of Biochemistry, University of Lund, P.O. Box 740, S-220 07, Lund 7, Sweden; and ‡Department of Chemistry, Temple University, Philadelphia, Pennsylvania 19122

Communicated by Joseph S. Fruton, October 2, 1978

**ABSTRACT** X-ray crystallographic data show that a specific tetrapeptide aldehyde inhibitor (*N*-acetylprolylalanylprolyl-phenylalaninal) forms a stable, covalent, tetrahedral addition complex with the serine protease, SGPA, from *Streptomyces griseus*. Earlier proposals, based on kinetic measurements, for the covalent nature of such linkages are confirmed, and the difference electron density map of this aldehyde inhibitor indicates that a major conformational change of the histidyl-57 side chain occurs on inhibitor binding.

Peptide aldehyde analogs of good substrates have been shown to be very strong competitive inhibitors of serine and cysteine proteases (1-6). Indeed, under similar conditions specific peptide aldehydes bind much more strongly to these enzymes than other analogous peptide inhibitors and substrates. The tendency of aldehydes to form tetrahedral adducts in aqueous solution and the expected proximity of a nucleophilic group in the enzyme's active site suggest that the complex formed by a peptide aldehyde with a serine or cysteine protease is covalent. The stability of such an adduct would therefore be due to the stability of the covalent "intramolecular" hemiacetal bond (3). The similarity of the chemical linkage of aldehyde adducts to the proposed tetrahedral intermediate on the reaction pathway of true substrates suggests that stabilization of such tetrahedral species is also largely a result of the covalent nature of the intramolecular bond (7-9).

To establish unequivocally the nature of peptide aldehyde complexation in the active sites of serine proteases, we have collected kinetic data and 2.8-Å resolution crystallographic data from the complex of *Streptomyces griseus* protease A (SGPA) with the specific peptide aldehyde Ac-L-Pro-L-Ala-L-Pro-L-Phe-H (C<sub>24</sub>H<sub>32</sub>O<sub>5</sub>N<sub>4</sub>), in which the phenylalanine residue has an aldehyde function in place of a carboxyl group. The selection of this peptide aldehyde was governed by the specificity of subsite S1 (10) of SGPA for Phe, Tyr, and Leu residues (11). In addition, earlier observations suggested that peptides incorporating the sequence Pro-Ala-Pro (P<sub>4</sub> - P<sub>2</sub>) bind in only one mode on the surface of SGPA (11). In the following discussion we will show that the complex of SGPA with this peptide aldehyde is a covalent one and that an active site residue in the complex is perturbed from its position in the native enzyme.

**Kinetic and Crystallographic Data Collection.** The SGPA preparation used for kinetic studies has been described (12). SGPA is identical to *S. griseus* protease 3 (SGP3) of Bauer and Löfqvist (12). The synthesis of the peptide aldehyde has been reported (13). Inhibition of SGPA-catalyzed hydrolysis of Ac-Pro-Ala-Pro-Phe-NH<sub>2</sub> (pH 9.00) and of Ac-Pro-Ala-Pro-Phe-

OMe (pH 4.00) by Ac-Pro-Ala-Pro-Phe-H (pH 4.00 and 9.00) and Ac-Pro-Ala-Pro-Phe-NH<sub>2</sub> (pH 4.00) was followed in a pH-stat at 37°C (11). *K<sub>i</sub>* values were determined from Dixon (14) or Henderson (15) plots.

Isolation, purification, and the subsequent crystallization of SGPA at pH 4.1 were carried out as described (16, 17). A suitable crystal of the SGPA-peptide aldehyde complex was prepared by immersing a native SGPA crystal into an ≈1 mM peptide aldehyde solution containing 1.5 M NaH<sub>2</sub>PO<sub>4</sub> at pH 4.1. The rate of peptide aldehyde penetration could be conveniently followed as a function of the change in refractive index of the crystal as monitored under cross-polarized light in a petrographic microscope.

Upon completion of this soaking procedure (≈6 hr), 2.8-Å resolution x-ray diffractometer data were collected and processed as described (17). Structure factor amplitude differences observed between the diffraction data from the SGPA-peptide aldehyde complex and from native SGPA were used to compute a difference electron density map. The coefficients for this Fourier synthesis were the figure-of-merit-weighted differences  $|F_{P+A}| - |F_P|$ , in which  $|F_P|$  represents the structure factor amplitudes of the native SGPA and  $|F_{P+A}|$  represents those amplitudes from a crystal of the complex. The phases for this difference map were the 2.8-Å multiple isomorphous replacement protein phases (17). The relevant crystallographic data collection and processing statistics are shown in Table 1. This three-dimensional difference Fourier map was interpreted with the aid of a Richards optical comparator (18). Coordinates for all nonhydrogen peptide aldehyde atoms were measured from the resultant model and stereochemically fitted by using Diamond's (19, 20) model-building program.

**Kinetic Investigations.** Both Henderson and Dixon plots of the inhibition of SGPA-catalyzed hydrolysis reactions by Ac-Pro-Ala-Pro-Phe-H indicate that the aldehyde is a reversible, competitive inhibitor. The kinetic data of Table 2 show that the aldehyde binds ≈10<sup>4</sup>-fold tighter than the corresponding peptide amide at an optimal pH (9.00). The binding of the aldehyde and the amide have also been investigated at a nonoptimal pH (4.00), close to the pH used in the crystallographic investigation (4.1). On going from pH 9.00 to 4.00 there is a decrease in binding of the peptide amide to approximately 1/2. The binding of the peptide aldehyde is clearly much more pH dependent, there being a decrease to 1/40th in binding upon lowering the pH to 4.00. Still, the peptide aldehyde is a very efficient inhibitor, binding about 600-fold tighter to SGPA than the peptide amide at this acid pH. The tight binding of this specific aldehyde to SGPA, both at pH 4.00 and at pH 9.00, is

The publication costs of this article were defrayed in part by page charge payment. This article must therefore be hereby marked "advertisement" in accordance with 18 U. S. C. §1734 solely to indicate this fact.

Abbreviations: SGPA, *S. griseus* protease A; e, electron; -H at the right of an amino acid symbol indicates that the carboxyl group has been replaced by an aldehyde group.

Table 1. Diffraction data statistics

Data	Native enzyme	SGPA-aldehyde complex
$a = b, c, \text{\AA}$	55.14, 54.81	55.17, 54.62
Reflections measured	9165	4582
Maximal absorption correction, %	14.9	6.7
Maximal crystal decay, %	10.2	5.3
$R_{\text{sym}} = \left( \sum_i  \bar{I} - I_i  / \sum_i I_i \right), \%$	1.7	1.5
Reflections merged	4113	304
Reflections [ $I > 3\sigma(I)$ ], %	96.2	94.5
$R_D = \frac{\sum_{hkl}   F_{P+A}  -  F_P  }{\sum_{hkl}  F_P }, \%$	—	10.0

comparable to the binding of other specific peptide aldehydes to elastase (3).

**Difference Map Interpretation.** The difference-electron density in the region of the active site of SGPA is illustrated in Fig. 1A, with the interpretation of that electron density shown below, in terms of a model in Fig. 1B. Comparison of these two portions of Fig. 1 show that the main details of the difference electron density are explained by the model of the bound tetrapeptide aldehyde that we have derived. In addition, this difference map shows that there is a major conformational change in the SGPA molecule that takes place on forming the aldehyde complex. This change is seen as the large positive and negative peaks just to the left (in this figure) of the main portion of the difference electron density representing the bound peptide aldehyde. The position of the His-57 side chain in the native enzyme is the negative peak (labeled His<sub>n</sub> in Fig. 1A), and this side chain moves to the new position in the aldehyde complex that is coincident with the positive peak labeled His<sub>a</sub>. Clearly, a major disruption of this active site residue has taken place.

Another important feature of the difference map of Fig. 1A is the fact that the difference electron density associated with the peptide aldehyde is continuous with that electron density of the native enzyme O $\gamma$  position of the active site residue Ser-195. This is more clearly shown in Fig. 1C, which shows a portion of the  $2|F_{P+A}| - |F_P|, \alpha_P$  electron density map about the bond between the  $\gamma$  oxygen of Ser-195 and the aldehyde carbon atom. The continuous electron density in Fig. 1C is conclusive evidence of the covalent nature of the linkage between this specific peptide aldehyde and SGPA. There are also a number of smaller positive and negative peaks in the region

Table 2. Kinetic data for peptide amide and aldehyde

Peptide	pH	$K_i, M$	$K_m, M$
Ac-Pro-Ala-Pro-Phe-NH <sub>2</sub>	9.00		$5.4 \times 10^{-4}^*$
	4.00	$1.2 \times 10^{-3}\dagger$	
Ac-Pro-Ala-Pro-Phe-H	9.00	$5 \times 10^{-8}$	
	4.00	$2 \times 10^{-6}$	

\* It has been shown that the  $K_m$  of this peptide amide can be equated with its  $K_S$  (11).

† It is not possible to determine a  $K_m$  at this low pH due to a decrease in catalytic activity to less than 1/100th (21) and an unsuitable pH for titration of amide hydrolysis (22). Instead we have determined the  $K_i$  of the amide.

of the difference density shown in Fig. 1A. The positive peaks can be attributed to new positions of bound solvent (i.e., water molecules) in the aldehyde crystals, whereas the negative peaks represent the positions of solvent molecules that have been displaced from the native enzyme upon complex formation with the aldehyde.

To show how the peptide aldehyde interacts with the enzyme SGPA we have included in Fig. 2A, for comparison, our interpretation of the 2.8- $\text{\AA}$  resolution electron-density map of the active site region of the native protein (24). Those portions of polypeptide chain making up the active site region of SGPA and, in particular, the four major catalytic residues, Ser-214, Asp-102, His-57, and Ser-195, have conformations similar to those of other serine proteases (24). A stereo drawing of the 2.8- $\text{\AA}$  resolution model of the peptide aldehyde bound to this active site region of SGPA is shown in Fig. 2B. It can be seen from these two figures that there are a number of intermolecular contacts involving both hydrogen-bonding and van der Waals interactions in addition to the covalent bond from the aldehyde carbonyl carbon atom to O $\gamma$  of Ser-195.

The primary specificity pocket of SGPA is defined by three regions of the molecule: the polypeptide chain from Ala-192 to Pro-192B, the polypeptide chain from Gly-215 to Gly-218, and residues Thr-226 and Phe-227. Hydrophobic interactions of these regions with the P1 Phe residue (P indicates position in the peptide) are evident in Fig. 2B. Another hydrophobic pocket can be discerned in the region of the phenyl ring of Tyr-171, the imidazole ring of His-57, and sections of the main chain in the vicinity of Ser-174. This second surface depression, which one can designate as S2, forms the binding pocket for the P2 Pro residue of the inhibitor. An almost identical conformation of residues forming this S2 subsite in the enzyme SGPB (25) is responsible for the markedly enhanced rate of inhibition by peptide chloromethyl ketones that have hydrophobic P2 side chains (26). As shown in Fig. 2B, the side chain of P3 Ala does not interact with the enzyme surface and is oriented into surrounding solvent. The terminal Ac-Pro moiety (P4-P5) of the aldehyde inhibitor is well resolved in the electron density map (Fig. 1), but nevertheless lies in a less-well-defined site that is primarily of hydrophobic character, with the major contacts between enzyme and inhibitor involving the side chains of Val-169, Tyr-171, and parts of the main polypeptide chain at residues Gly-216 and Ser-217.

There are five hydrogen bonds between SGPA and the aldehyde inhibitor, all of which involve only main polypeptide chain atoms of SGPA. Three of these hydrogen bonds result in an approximate antiparallel  $\beta$ -sheet conformation between the inhibitor P1 Phe and P3 Ala and the enzyme residues Ser-214 and Gly-216. Similar interactions have been described for specific chloromethyl ketone inhibitors of  $\gamma$ -chymotrypsin (27) and subtilisin (28, 29). Formation of these three hydrogen bonds is accompanied by a small reorientation of the carbonyl oxygen atoms of Ser-214 and Gly-216. These minor conformational changes are not indicated in Fig. 2B.

The other two hydrogen bonds involve the aldehyde carbonyl oxygen atom and the two peptide NH groups of Gly-193 and Ser-195. Unlike the interactions described above, this interaction may change appreciably during the catalytic process as the substrate proceeds from a carbonyl group to an alkoxide anion or alcohol and back to a carbonyl group. This interaction will also be clearly affected by the changing geometry of the carbon atom of the susceptible peptide bond. Interactions within this binding site, known as the oxyanion hole (28), are therefore likely to be of importance in reducing the free energy of activation for hydrolysis.

Our interpretation of the electron density map of Fig. 1A and C puts the aldehyde carbonyl carbon atom within covalent

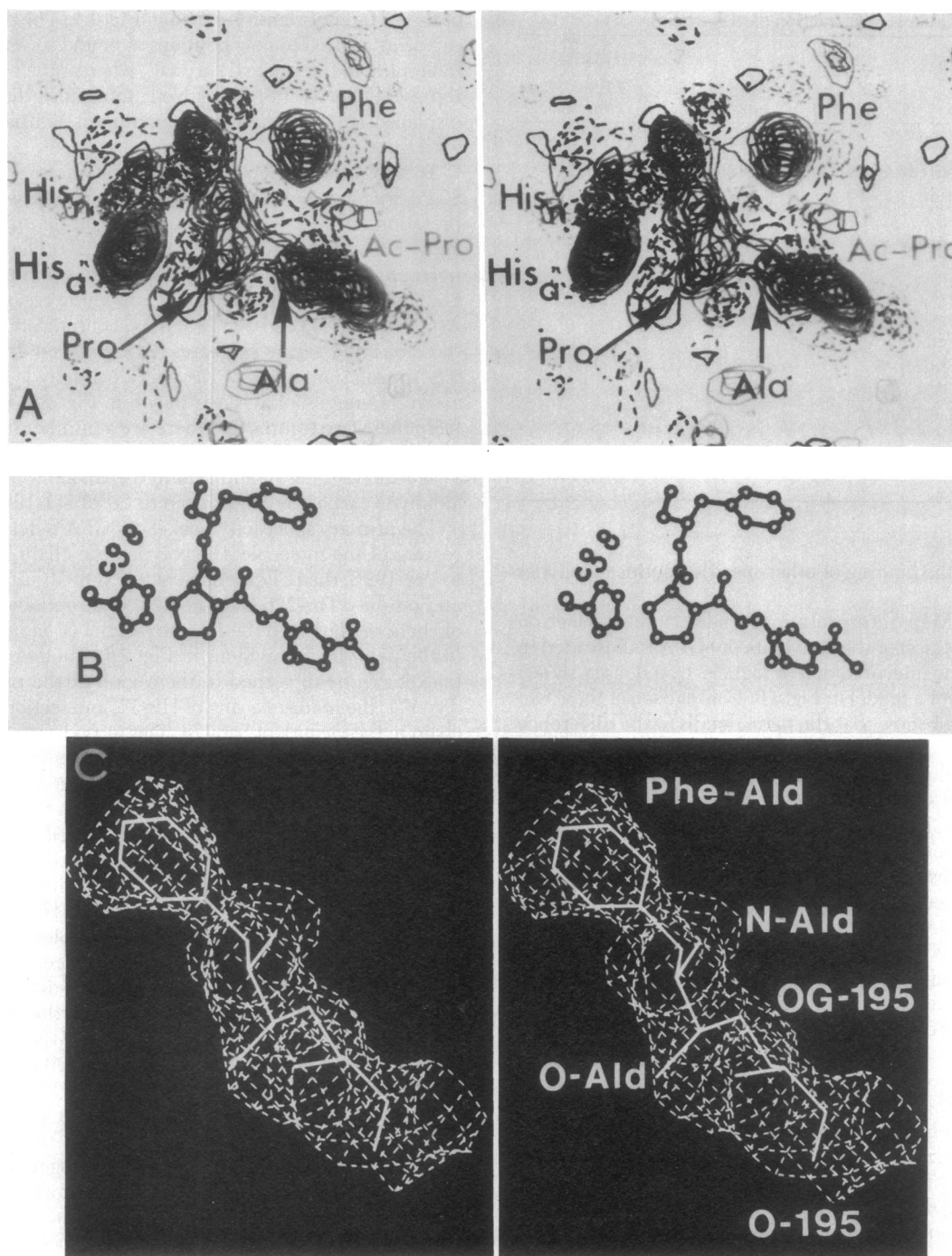


FIG. 1. (A) Stereo representation of the difference Fourier electron density map of the SGPA-peptide aldehyde complex at 2.8-Å resolution through the region of the enzyme containing the active site. The view presented is directly down the *c* axis of the unit cell. The standard error (23) of this map was estimated to be 0.029 electron ( $e/\text{Å}^3$ ). The first contour level has been drawn at  $\pm 0.066 e/\text{Å}^3$ , with subsequent contours drawn at increasing intervals of  $0.033 e/\text{Å}^3$ . The highest difference electron density peak is  $\approx 13\sigma$  above background. (B) Stereo drawing of the idealized Kendrew-Watson model interpretation of the difference electron density of the SGPA-peptide aldehyde complex. The native enzyme position of the side chain of His-57 is indicated by those atoms drawn for which connective bonds are absent. (C) Stereo representation of a portion of the electron density map in the region of the covalent bond between the active site residue Ser-195 and the phenylalaninal residue of the bound aldehyde inhibitor. This electron density map was calculated using as coefficients  $2|F_{P+A}| - |F_P|$ , with the phases  $\alpha_P$ . The broken contour envelopes are drawn at  $0.34 e/\text{Å}^3$  [including  $0.23 e/\text{Å}^3$  contributed by the  $F(000)$  term]. The atomic model is drawn with solid lines and some of the atoms present have been labeled: Ald, aldehyde; OG,  $\gamma$  oxygen. This photograph was produced by using the MMS-X graphics system.

bond distance of O $\gamma$  of Ser-195 ( $\approx 1.5 \text{ Å}$ ). No movement of the O $\gamma$  atom from its native position is observed on the binding of the aldehyde. Fig. 2B shows the environment of the aldehyde carbonyl oxygen atom along with the two hydrogen bonds formed to the amide nitrogen atoms of Gly-193 and Ser-195. In addition, there are two reasonably well-ordered solvent molecules (tentatively interpreted as H<sub>2</sub>O) and labeled W1 and

W2 in Fig. 2B, one of which is within hydrogen-bonding distance of this carbonyl oxygen atom.

The binding of this tetrapeptide aldehyde displaces a number of well-ordered solvent molecules (herein assumed to be water molecules) from the surface of SGPA, as evidenced from this difference map (Fig. 1A). The map of native SGPA has a solvent molecule that coincides with the position of the C $\gamma$  atom

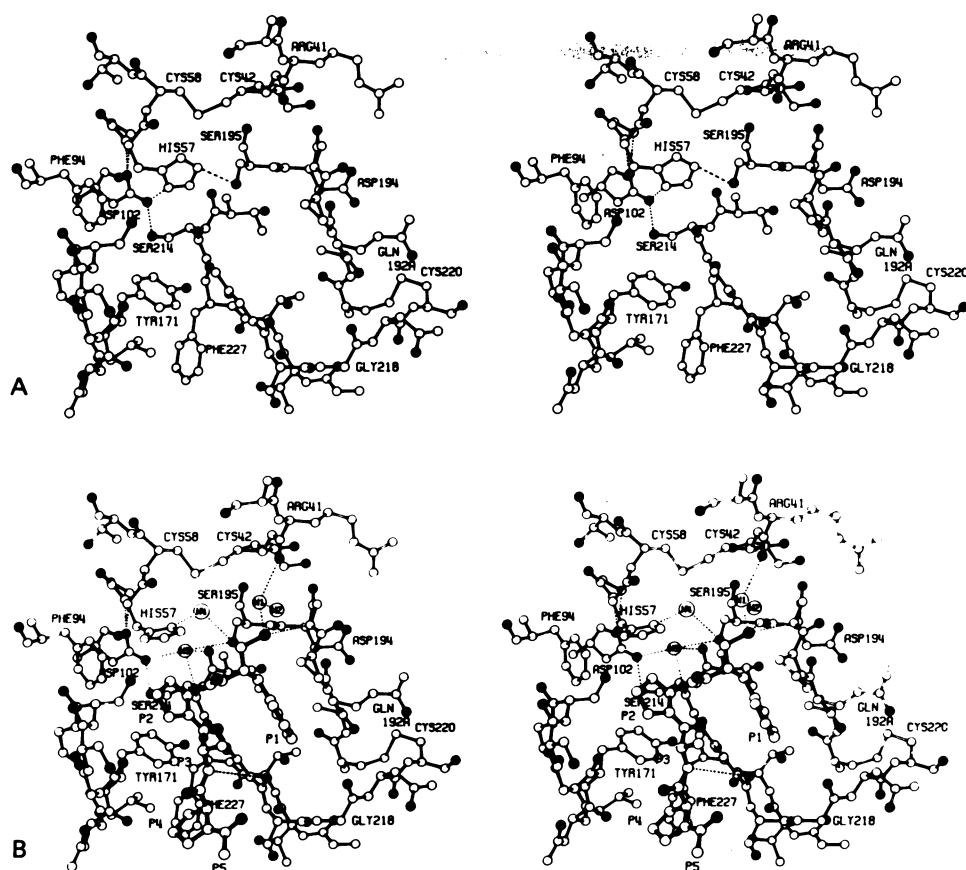


FIG. 2. (A) Stereo drawing of the active site region of SGPA as observed in the native enzyme structure at 2.8-Å resolution. The polypeptide main chain bonding is shown with filled black bonds and oxygen atoms are distinguished by filled black circles. Hydrogen bonds between active site residues and surrounding polypeptide chains have been illustrated as broken lines. (B) Stereo drawing of the SGPA-peptide aldehyde complex as determined from the 2.8-Å resolution difference electron density map. Polypeptide main chain bonding of the enzyme is shown with filled black bonds, as are all interatomic bonds of the bound peptide aldehyde. All oxygen atoms present are distinguished by filled black circles. Hydrogen bonds are indicated by broken lines. The new position of the side chain of His-57 in the complex is also drawn. Solvent molecules bound upon peptide-aldehyde complexation are indicated by the symbols W1-W4.

of the P1 Phe residue, thus explaining the weak density connecting the phenyl ring of this Phe to the  $\alpha$  carbon atom. A second water molecule is displaced near the *para* position of this Phe (Fig. 1A). The P2 Pro residue displaces a solvent peak that is close to the main-chain carbonyl oxygen atom of Ser-214. There are a number of less well-defined solvent peaks that have been displaced by the Ac-Pro moiety.

In addition to the two solvent molecules, W1 and W2, that are bound to the SGPA-aldehyde complex, two other water molecules, W3 and W4, are located in the active site region. Water W3 is situated near the original native position of the imidazole ring of His-57, making close contacts to Asp-102, to the carbonyl oxygen atoms of Thr-213 and Ser-214, and to the  $O^\gamma$  of Ser-195. It is clear from Fig. 2B that the carboxylate of Asp-102 has been exposed to solvent upon the movement of the imidazole ring of His-57. The fourth water molecule W4 makes hydrogen-bonding interactions with  $N^{\delta 1}$  of His-57 at its new position and  $O^\gamma$  of Ser-195.

**Aldehydes as Transition State Analogues.** The peptide aldehyde used in this study binds to SGPA several orders of magnitude more tightly than the corresponding peptide amide, both at pH 9.00 and at pH 4.00. According to transition state theory (7), this is consistent with the peptide aldehyde-SGPA complex being an analogue of the peptide amide-SGPA transition state complex. The binding modes of both nonspecific and specific peptide aldehydes to serine proteases have been discussed by several authors (3, 4, 30, 31). In principle, two alternative binding modes have been suggested: (i) covalent bond formation between the aldehyde carbon atom and the active site Ser-195 oxygen atom, or (ii) noncovalent interactions between the peptide aldehyde (or hydrate) and the active site of the enzyme.

The x-ray crystallographic results presented above represent the structural determination of an enzyme-peptide aldehyde

complex. These results (as depicted in Fig. 1C) present direct visual evidence that a stable covalent tetrahedral hemiacetal adduct is formed by a specific peptide aldehyde in the active site of a serine protease. Indeed, inspection of the difference electron density map of this complex and its subsequent interpretation places the aldehyde carbon atom of the bound peptide  $\approx 1.5$  Å from the  $\gamma$  oxygen atom of Ser-195 in the active site of SGPA. This covalent interaction and other noncovalent aldehyde to enzyme interactions are summarized in the stylized drawing of Fig. 3.

Another important feature of the SGPA-peptide aldehyde complex is the reorientation of the side chain of the active site residue His-57. This is achieved via two rotations: one of  $94^\circ$  about its  $C^\alpha-C^\beta$  bond and another at  $26^\circ$  about the  $C^\beta-C^\gamma$

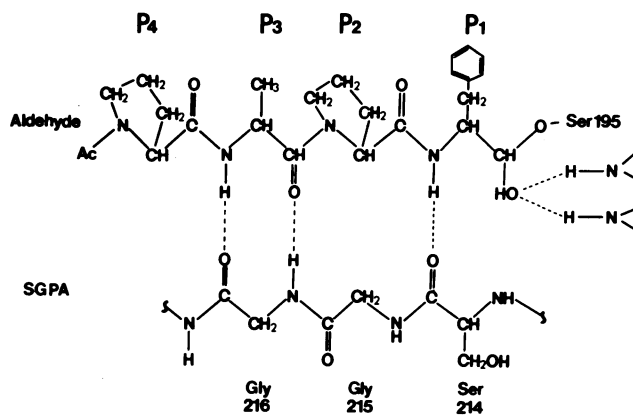


FIG. 3. Interactions between the bound peptide aldehyde and SGPA. Along with the covalent bond formed to the  $\gamma$  oxygen atom of Ser-195, five hydrogen bonds are formed with surface enzyme groups. Three of these hydrogen bonds taken on approximate anti-parallel  $\beta$ -sheet conformation.

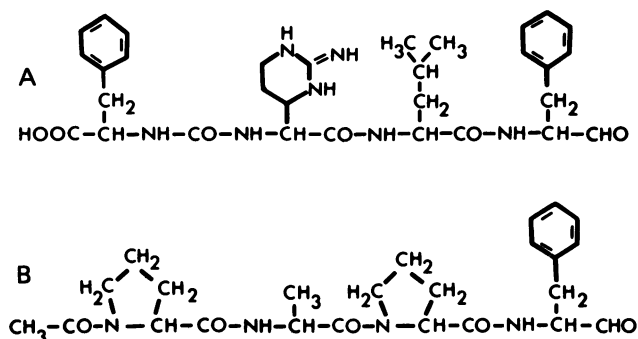


FIG. 4. Structural comparison of chymostatin-A (A), a naturally occurring peptide aldehyde, and the peptide aldehyde (B) complexed with SGPA in this study. Both of these peptides have a COOH-terminal phenylalanine residue.

bond. The possibility of His-57 rearrangement in the active sites of serine proteases upon peptide-aldehyde complexation has been postulated (5) in a paper describing an NMR study of the microbial serine protease  $\alpha$ -lytic protease. Recent sequence and structural studies (32, 33) of  $\alpha$ -lytic protease have shown that this enzyme is highly homologous to SGPA and has a very similar disposition of active site residues.

Like SGPA,  $\alpha$ -lytic protease binds a specific peptide aldehyde much tighter than the corresponding peptide alcohol and methyl ester (5). NMR analysis of the complex formed by  $\alpha$ -lytic protease and the peptide aldehyde Ac-Ala-Pro-Ala-H below pH 5.0 suggests that a hemiacetal tetrahedral addition complex is formed and the presence of a protonated imidazole cation with considerable mobility is detected. The particular histidine involved is His-57, the only such residue in the polypeptide sequence. These results are directly comparable to the expulsion of His-57 into solvent in the SGPA-peptide aldehyde complex at pH 4.1. As has been observed for native SGPA, further NMR analysis of native  $\alpha$ -lytic protease between pH 3.5 and 6.0 indicates His-57 remains tightly lodged in the active site. Clearly His-57 mobility is a function of peptide-aldehyde complexation under pH 5.0.

NMR analysis of the  $\alpha$ -lytic protease-peptide aldehyde complex above pH 7.0 indicates His-57 retains its native conformation upon hemiacetal formation (5). Lowering the pH from 7.0 to 5.5 results in the acquisition of a proton by His-57 and another by either the aldehyde oxygen of the hemiacetal complex or by the carboxyl group of Asp-102. These results suggest a reorientation of the tetrahedral hemiacetal addition complex takes place upon lowering pH, which is responsible for the ejection of His-57 from the active site. Such an explanation is consistent with the present SGPA-peptide aldehyde complex model at pH 4.1 (Fig. 2B), which places the bound aldehyde carbon atom only 2.9 Å from the native position of the side chain of His-57, with the aldehyde hydrogen oriented even closer by the solvated position of the aldehyde oxygen in the oxyanion hole. If the model is adjusted so that the aldehyde oxygen is optimally positioned in the oxyanion hole, as would be expected at pH > 7.0, where SGPA is most catalytically active, these prohibitive contacts are relieved. A similar movement of the His-57 residue of the microbial serine protease-SGPA has also been observed for steric reasons resulting from a covalently bound pipsyl group on Ser-195 (34).

The present study also serves to explain the mode of activity of naturally occurring peptide aldehydes, which have been isolated from several strains of *Streptomyces* (35). These peptide aldehydes are also effective serine protease inhibitors, with

high binding constants. A comparison of one such peptide aldehyde, chymostatin-A, and the peptide aldehyde used in this study is shown in Fig. 4. Chymostatin-A, like the peptide aldehyde complexed to SGPA, has a COOH-terminal phenylalanine residue and is specific for chymotryptic-like serine proteases such as SGPA (36).

This work is supported by a grant from the Medical Research Council of Canada to the Medical Research Council Group on Protein Structure and Function at the University of Alberta and a grant to R.C.T. from Merck, Sharp and Dohme. C.-A.B. thanks the Royal Physiographic Society and The Swedish Natural Science Research Council for a research and travel grant.

1. Westerik, J. & Wolfenden, R. (1972) *J. Biol. Chem.* **247**, 8195-8197.
2. Ito, A., Tokawa, K. & Shimizu, B. (1972) *Biochem. Biophys. Res. Commun.* **49**, 343-349.
3. Thompson, R. C. (1973) *Biochemistry* **12**, 47-51.
4. Breau, E. S. & Bender, M. L. (1975) *FEBS Lett.* **56**, 81-84.
5. Hunkapiller, M. W., Smallcombe, S. H. & Richards, J. H. (1975) *Org. Mag. Reson.* **7**, 262-265.
6. Clark, P. I., Lowe, G. & Nurse, D. (1977) *J. Chem. Soc. Chem. Commun.* 451-453.
7. Wolfenden, R. (1972) *Acc. Chem. Res.* **5**, 10-18.
8. Wolfenden, R. (1976) *Annu. Rev. Biophys. Bioeng.* **5**, 271-306.
9. Lienhard, G. E. (1973) *Science* **180**, 149-154.
10. Schechter, I. & Berger, A. (1967) *Biochem. Biophys. Res. Commun.* **27**, 157-162.
11. Bauer, C.-A., Thompson, R. C. & Blout, E. R. (1976) *Biochemistry* **15**, 1291-1295.
12. Bauer, C.-A. & Löfqvist, B. (1973) *Acta Chem. Scand.* **27**, 3147-3166.
13. Thompson, R. C. (1977) *Methods Enzymol.* **46**, 220-225.
14. Dixon, M. (1953) *Biochem. J.* **55**, 170-171.
15. Henderson, P. J. F. (1972) *Biochem. J.* **127**, 321-333.
16. Jurásek, L., Johnson, P., Olafson, R. W. & Smillie, L. B. (1971) *Can. J. Biochem.* **49**, 1195-1201.
17. Brayer, G. B., Delbaere, L. T. J. & James, M. N. G. (1978) *J. Mol. Biol.* **124**, 243-260.
18. Richards, F. M. (1968) *J. Mol. Biol.* **37**, 225-230.
19. Diamond, R. (1966) *Acta Crystallogr.* **21**, 253-266.
20. Diamond, R. (1974) *J. Mol. Biol.* **82**, 371-391.
21. Bauer, C.-A. & Petterson, G. (1974) *Eur. J. Biochem.* **45**, 469-472.
22. Kurtz, A. N. & Niemann, C. (1962) *Biochemistry* **1**, 238-243.
23. Henderson, R. & Moffat, J. K. (1971) *Acta Crystallogr. Sect. B* **27**, 1414.
24. Brayer, G. B., Delbaere, L. T. J. & James, M. N. G. (1978) *J. Mol. Biol.* **124**, 261-282.
25. Delbaere, L. T. J., Hutcheon, W. L. B., James, M. N. G. & Thiessen, W. E. (1975) *Nature (London)* **257**, 758-763.
26. Gertler, A. (1974) *FEBS Lett.* **43**, 81-85.
27. Segal, D. M., Powers, J. C., Cohen, G. H., Davies, D. R. & Wilcox, P. E. (1971) *Biochemistry* **10**, 3728-3737.
28. Robertus, J. D., Alden, R. A., Birktoft, J. J., Kraut, J., Powers, J. C. & Wilcox, P. E. (1972) *Biochemistry* **11**, 2439-2449.
29. Paulos, T. L., Alden, R. A., Freer, S. T., Birktoft, J. J. & Kraut, J. (1976) *J. Biol. Chem.* **251**, 1097-1103.
30. Schultz, R. M. & Cheerva, A. C. (1975) *FEBS Lett.* **50**, 47-49.
31. Gorenstein, D. G., Kar, D. & Momii, R. K. (1976) *Biochem. Biophys. Res. Commun.* **73**, 105-111.
32. Johnson, P. & Smillie, L. B. (1974) *FEBS Lett.* **47**, 1-6.
33. James, M. N. G., Delbaere, L. T. J. & Brayer, G. D. (1978) *Can. J. Biochem.* **56**, 396-402.
34. Coddling, P. W., Delbaere, L. T. J., Hayakawa, K., Hutcheon, W. L. B., James, M. N. G. & Jurásek, L. (1974) *Can. J. Biochem.* **52**, 208-220.
35. Umezawa, H. (1976) *Methods Enzymol.* **45**, 678-695.
36. Tatsuta, K., Mikami, N., Fujimoto, K., Umezawa, S., Umezawa, H. & Aoyagi, T. (1973) *J. Antibiot.* **26**, 625-646.